Article:
Xi, Z., He, X., Wu, Z. et al. (2023) A rapid one-step preparation method of the repairable three-dimensional antifouling superhydrophobic 2.5EPZF coating on magnesium alloys. Surfaces and Interfaces, 42 (Part B). 103476. ISSN: 2468-0230

https://doi.org/10.1016/j.surfin.2023.103476

A rapid one-step preparation method of the repairable three-dimensional antifouling superhydrophobic 2.5EPZF coating on magnesium alloys

Zhongxian Xi[a,b], Xiaoyan He[a,b], Zumin Wu[a,b], Chengqing Yuan[a,b,*], Chun Wang[c]

a Reliability Engineering and New Energy Institute, School of Transportation and Logistics Engineering, Wuhan University of Technology, Hubei, 430063, China

b National Engineering Research Center for Water Transport Safety, Wuhan University of Technology, Hubei, 430063, China

c Institute of Functional Surfaces, School of Mechanical Engineering, University of Leeds, Leeds LS2 9JT, United Kingdom

*Corresponding author. *E-mail: ycq@whut.edu.cn (Chengqing Yuan)*

Abstract:

Although three-dimensional (3D) superhydrophobic coating has been gradually prepared on the surface of metal substrate for anticorrosion and antifouling, their complex preparation steps and equipment requirements limit their practical application. Herein, by a rapid one-step spray preparation method the fabricating 3D superhydrophobic 2.5EPZF (2.5 g epoxy resin/polycaprolactone (PCL)/zinc oxide/perfluorodecyltriethoxysilane) coating is prepared. This method utilizes a certain

degree of directional arrangement of macromolecular long chain polymers (PCL) as solvent evaporation during the spraying process to form a filamentous structure to construct the 3D coating. This preparation mechanism provides us a novel theoretical guidance method for preparing 3D coating. Further, the silk thickness and mesh density of the 3D mesh structure is controlled by adding epoxy resin. When the amount of epoxy resin is 2.5 g, the surface of 2.5EPZF coating is with about 1-3 μm thick branch frame and 0.1-0.4 μm thin treetop. And the water-contact angle (CA) of 2.5EPZF is 156.6 ± 1.5° and the sliding angle (SA) is < 10° . The 2.5EPZF coating exhibits durable antifouling, strong mechanical&chemical durability, and corrosion resistance. The corrosion current of the 2.5EPZF coating for 0 day's immersion and 35 days' immersion in NaCl solution is 1.043 x 10^{-12} A•cm^{-2} and 1.1703 x 10^{-11} A•cm^{-2}, respectively. Under solar irradiation and at 50 °C for 30 min, the 2.5EPZF coating is with scratching recovering. Additionally, the composite coating can be prepared by a large area. It is expected that this method is readily used and shows great application potentials.

Keywords: PCL, Epoxy, Magnesium alloys, three-dimensional coating, superhydrophobic, anticorrosion and antifouling

1. Introduction

As a solar irradiation structural metal material, magnesium alloys have been widely used in automation industry, ship and automobile, aerospace, missile vehicle, electronic and electrical appliances, etc., due to its outstanding physical and mechanical properties, non-magnetic properties and good thermal dissipation [1-11]. In the field of marine automobile, magnesium alloys are used as instrument panel, steering wheel, gearbox, oil sump, gear box, cylinder cover, seat frame, deck and some wheel hubs, special vessels such as small investigation and experiment ships use magnesium alloys as the hull shell structure and so on [12-18]. However, the poor corrosion resistance of magnesium alloys, especially in the sea environment containing chloride ions, limits the application of magnesium alloys as solar irradiationweight materials for medium and large ships [19-22].

At present, the superhydrophobic coating prepared by one-step method usually was the two-dimensional (2D) coating, such as the epoxy resin (EP)/polymethylhydrosiloxane (PMHS)/modified nano-SiO_2 layer [23], the Maleic anhydride (MAH)/Epoxy resin grafted with fluorine containing side chains (FEP) coating [24], Epoxy resin (EP)/Polydimethylsiloxane (PDMS)/SiO_2 coating [25], and

so on. The stability of the superhydrophobic coating maintains the continuous air film to prevent the invasion of the corrosive media. Compared with 2D coating, the hydrophobic coating with three-dimensional (3D) micropore structure could anchor the air film more tightly in dynamic condition. The current creation of materials with 3D structures often adopts multi-step method (the preparation of fluffy ZnO rods/PDMS by spraying, hydrothermal method and modified by 1H,1H,2H,2H-perfluorooctyltriethoxysilane [26]), sophisticated and special equipment, such as template method, foaming method, adding primary structural particles of specific shape (nanotube, filamentous, needle-shaped, four-corner needle-shaped, etc.), or adopting electrostatic spinning (the preparation of PCL/MSO/SiO_2 hierarchical superhydrophobic mats [27] and Polydimethylsiloxane (PDMS)-modified PCL membranes by electrospinning [28]), 3D printing, optical or laser etching [29-32]. These preparation methods are complicated in steps and long in cycle, or utilize special equipment with high requirements for electrospinning machines, 3D printers, lithography machines and other equipment, which is not convenient for large-area preparation, and is limited by the special structure and shape of the matrix, which is not conducive to large-scale promotion and application [30, 33, 34].

This work explores the use of the simple one-step spray method to generate three-dimensional reticulated porous 2.5EPZF composite coating on magnesium alloy substrate.

PCL, as a semi-crystalline non-toxic biodegradable polymer, is widely used in food packaging, drug release materials, biological implant materials and so on because of its certain hydrophobicity, excellent rheological properties and considerable toughness [22,35]. PCL can form three-dimensional reticulated and porous coating by spraying as a forming component. Epoxy resin (EP) is a thermosetting resin with excellent overall performance. It has good adhesion performance, outstanding corrosion resistance, excellent chemical resistance, low shrinkage characteristics, easy to process and low costs to be widely used in coating, adhesives and other fields [36-38]. Herein, the epoxy resin is as a molding control function, which can control the pore size and porosity of the three-dimensional network structure. Zinc oxide (ZnO) nanoparticles have the characteristics of safety, non-toxicity, high stability, strong photoelectric performance and good antibacterial activity, which are widely used in optoelectronic devices, environmental remediation, food packaging, coating rubber and other industries [39-41]. In this work, ZnO nanoparticles play an essential role in the

construction of micro-nano structure and the attachment of low-surface energy substances, improving the coating roughness and facilitating the uniform distribution of low-surface energy substances. 1H, 1H, 2H, 2H perfluorodecyltrichlorosilane (PFDTES) is a kind of fluorinated organic silane with low surface energy. In this paper, PFDTES is used to reduce the surface energy of materials, to improve the hydrophobicity and corrosion resistance of coating, and restrain the marine bacteria adhesion and fouling [42-45].

In this work, the superhydrophobic 2.5EPZF composite coating was prepared by one-step spraying method. The directional arrangement mechanization of macromolecular long chain polymers (PCL) as solvent evaporation during the spraying process to form a filamentous structure to construct provided a new preparation pathway to prepare the 3D coating. And this method could be used for large-scale 3D coating's preparation without the limitation of the substrate's shape.

2. Experimental Section

2.1. Materials

Dichloromethane (DCM) (Qingmei Chemical Reagent Factory, China), 1H,1H,2H,2H-perfluorodecyltriethoxysilane (PFDTES) (Guangzhou Hongcheng

Biotechnology Science and Technology Co., LTD, China, 97%), PCL (Mw: 80,000, Solvay Specialty Polymers, China), ZnO powders (30nm, Beijing Shenghehaoyuan Tech. Co. Ltd., China) and Die-cast AZ91D magnesium alloy (Dongguan Qingmei Metal Materials Co., Ltd., China) were used as the experimental materials. All chemicals were used without further modification.

2.2. Sample preparation

Die-casted Mg alloy (AZ91D) with a chemical composition (wt.) of 8.77% Al, 0.74% Zn, 0.18% Mn, 90.31% were cut into 50 mm x 25 mm x 5 mm. The samples were polished by silicon carbide papers from 150 to 1000 mesh. Then the samples were ultrasonically cleaned in acetone rinsed by de-ionized water, and dried at 60 ºC for the following coating preparation.

2.3. Preparation of composite coating

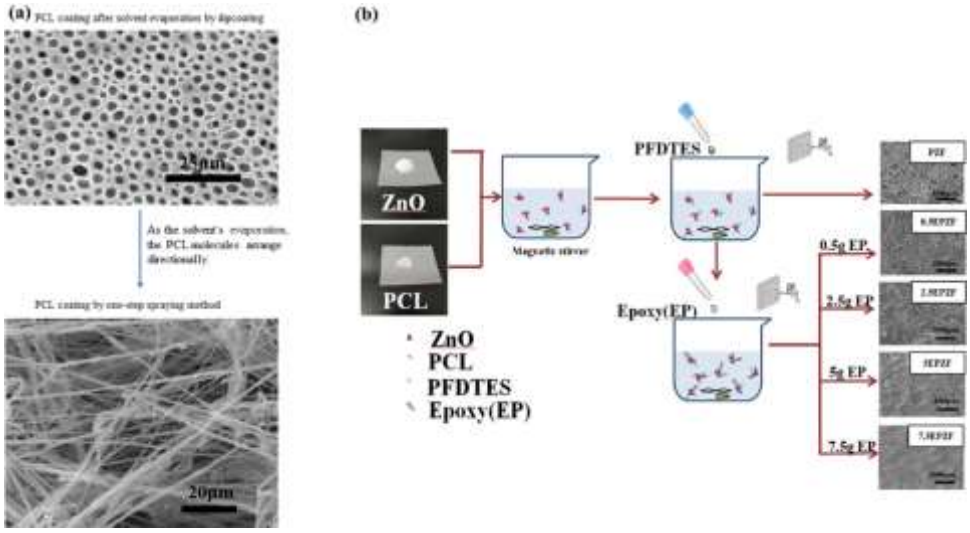

Scheme 1. The SEM of the PCL coating by dipcoating&spraying method (a) and the preparation process of the composite coating (b).

As shown in Scheme 1a, the PCL coating prepared by dipping would exhibit a regular multi-layernetwork structure in our former researches [46]. And we consided that the mechanism production of the regular network structure was the macromolecular long chain polymers (PCL) occurred a certain degree of directional arrangement during solvent evaporation. After multiple experiments, a three-dimensional network structure coating of PCL was prepared by simple spraying method as shown in Scheme 1a. By the same method, added ZnO nanoparticles (5 g, 6.14 x 10^{-2} mol), PFDTES (1 mL, 2.00 x 10^{-3} mol) to the PCL solution (PCL 5g, 6.25 x 10^{-5} mol, Dichloromethane (DCM, as the solvent), 80 mL) during the mixing process under vigorous stirring with a magnetic stirrer at RT as shown in Scheme 1b. Then, epoxy (EP) (0.5 g, 2.5 g, 5 g, 7.5 g) was added to the solution, respectively. The stirring process lasted for 1 hour. Then the polycaprolactone/epoxy resin/zinc oxide/perfluorodecyltriethoxysilane (EPZF) composite coating was prepared on the treated magnesium alloy substrate by one-step spray method under appropriate pressure with the stirred solution. After that, all samples were in the air at RT. for 24 h to dry and solidify. The PZF (polycaprolactone/zinc

oxide/perfluorodecyltriethoxysilane) coating was prepared by the same process as the control groups. The preparation conditions and the stirred solutions of samples with composite coating were shown in the table 1.

Sample	Stirred solutions	Preparation conditions
PZF	80 g DCM, 5 g PCL, 5 g ZnO, 1mL PFDTES	Room temperature 45 s
0.5EPZF	80 g DCM, 5 g PCL, 5 g ZnO, 1mL PFDTES, 0.5 g EP	
2.5EPZF	80 g DCM, 5 g PCL, 5 g ZnO, 1mL PFDTES, 2.5 g EP	
5EPZF	80 g DCM, 5 g PCL, 5 g ZnO, 1mL PFDTES, 5 g EP	
7.5EPZF	80 g DCM, 5 g PCL, 5 g ZnO, 1mL PFDTES, 7.5 g EP	

Table 1. The preparation conditions and the stirred solution of samples with composite coating.

2.4. Analysis of composite coating

The surface morphology of the prepared coating was observed by using scanning electron microscopy (SEM, VEGA3, Tescan Co. China Ltd., China) equipped with energy-dispersive spectrometer (EDS). The water contact angle (CA) was measured at room temperature using an optical contact angle meter (Dataphysics OCA 15EC, Germany) with a 5 μL water drop. Electrochemical tests were performed by electrochemical workstation (CorrTest CS350). The surface roughness of samples was measured by laser confocal microscope (CLSM) (VK-X1000, Keyence, Japan). The bacterial adhesion test was measured by using Bacillus subtilis CMCC (B) 63501 (Shanghai Luwei Technology Co., Ltd., China) at 120 rpm at 30 ºC for 20 days. Subsequently, the samples were observed by SEM and digital camera to measure the Bacillus adhesion status and the surface corrosion resistance features. Then, the FTIR analysis of the coating was measured by Thermoscientific (Summit Pro, USA). Further, the samples' mechanical adhesion, self-cleaning ability, abrasion resistance and pH

durability, Bacillus subtilis adhesion and Solar irradiation&thermal repair were measured in our study. Three parallel samples were measured in the test progress.

3. RESULTS AND DISCUSSION

3.1. Surface characteristics

The SEM surface morphology of PZF, 0.5EPZF, 2.5EPZF, 5EPZF, 7.5EPZF samples was shown in Figure 1. The coating of PZF (Figure 1a and b) and 0.5EPZF (Figure 1c and d) exhibited a three-dimensional surface with network structure and high porosity. With the addition of 0.5 g epoxy resin, the samples were with lower porosity and the ZnO particles were dispersed in network structure. Then with the increase of epoxy resin content, the 2.5EPZF (Figure 1e and f) sample was with spatial wire mesh-like skeleton structure and lower porosity. The diameter of mesh and skeleton of 2.5EPZF sample were about 0.1-0.4 μm and 1-3 μm. After that, with more addition of epoxy resin content, the network and porous structure of the 5EPZF (Figure 1g and h) and 7.5EPZF (Figure 1i and j) samples disappeared and the surface of 7.5EPZF samples became smooth.

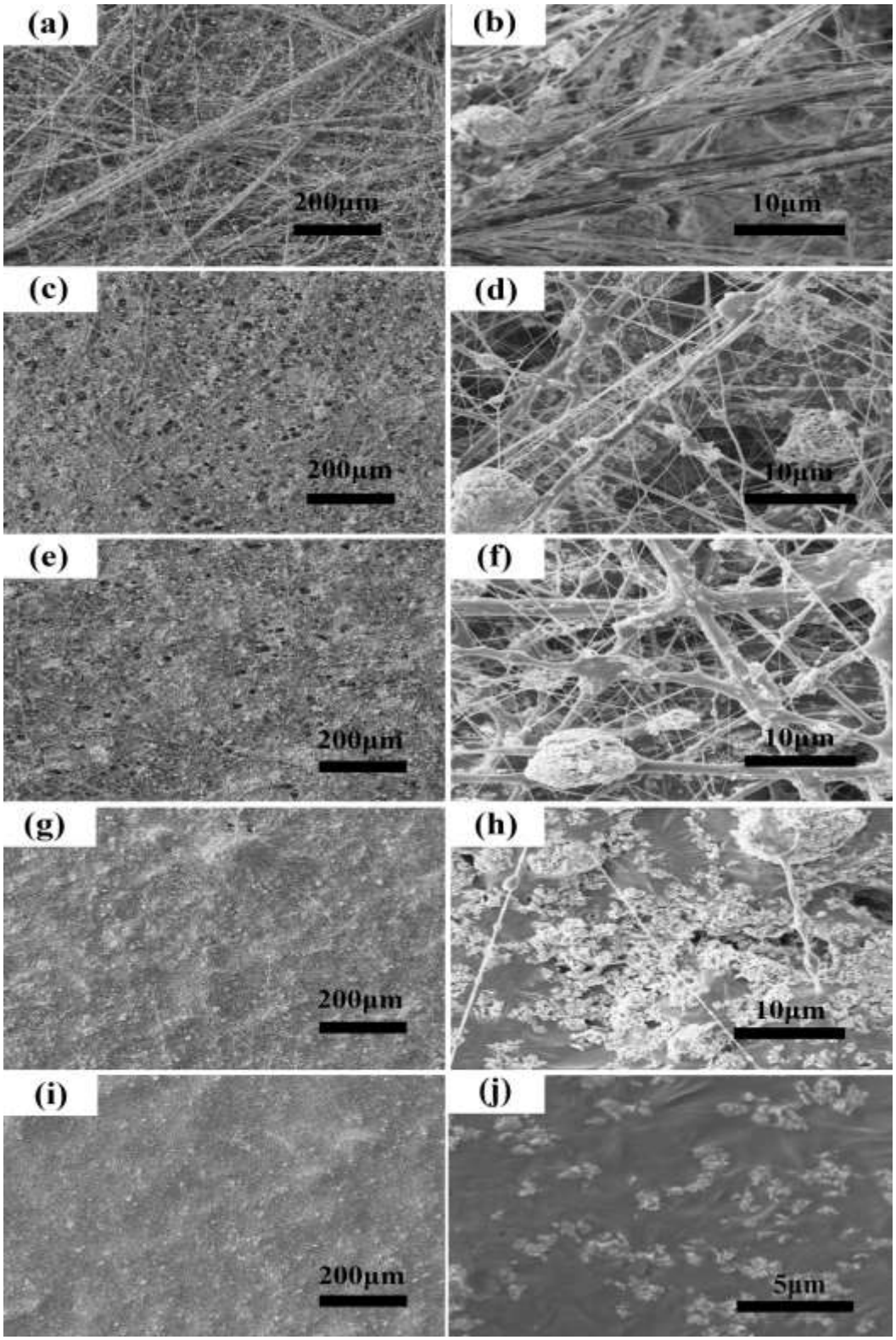

Figure. 1. The SEM images of PZF (a and b), 0.5EPZF (c and d), 2.5EPZF (e and f), 5EPZF (g and h), 7.5EPZF (i and j) samples.

The cross section SEM image of PZF (Figure 2a) and 0.5PZF (Figure 2b), 2.5EPZF (Figure 2c), 5EPZF (Figure 2d), 7.5EPZF (Figure 2e) samples were shown in Figure 2.

The thickness of PZF (Figure 2a) and 0.5PZF (Figure 2b), 2.5EPZF (Figure 2c), 5EPZF (Figure 2d), 7.5EPZF (Figure 2e) were about 137 μm, 178 μm, 77 μm, 84 μm and 108 μm, respectively. PZF and 0.5PZF samples were with three-dimensional network and porous structure. With the addition of 0.5 g EP, the coating thickness of 0.5EPZF (Figure 2b) sample was with significant increase. It was because the support force of the filamentous structure between layers increased under 0.5 g addition of EP. With the continue adding of EP content, the coating thickness of 2.5EPZF sample became thinner markedly to 77 μm (Figure 2c). And the reason was that the thin silk became thicker and the combination of filamentous structures between layers becomes tighter with 2.5 g EP addition. And then with the addition of 5 g EP and 7.5 g EP the thickness of composite coating gradually increased to 84 μm (Figure 2d) and 108 μm (Figure 2e). With the addition of 5g and 7.5 g EP, the network and porous structure of the 5EPZF and 7.5EPZF samples almost disappeared. When the addition of 5 g and 7.5 g EP could fully fill the pore, the thickness of the coating increased as the increasing amount of EP.

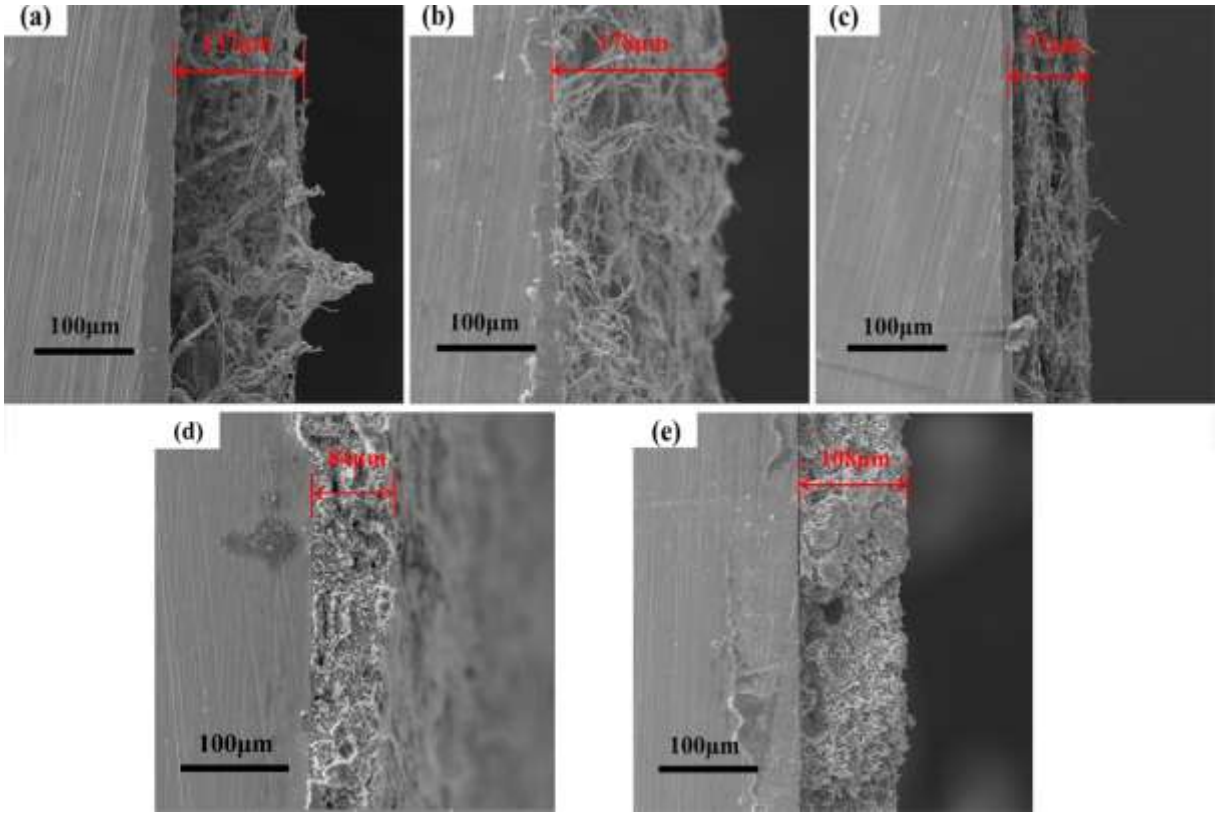

Figure. 2. The cross section SEM images of PZF (a) and 0.5EPZF (b), 2.5EPZF (c), 5EPZF (d), 7.5EPZF (e) samples.

3.2. Surface roughness characteristics

Moreover, roughness measurement with laser confocal microscope (VK-X1000, Keyence) and the 3D morphology of the samples of PZF (Figure 3a), 0.5PZF (Figure 3b), 2.5EPZF (Figure 3c), 5EPZF (Figure 3d), 7.5EPZF (Figure 3e) samples was shown in Figure 3. The surface roughness of PZF (Figure 3a) and 0.5PZF (Figure 3b), 2.5EPZF (Figure 3c), 5EPZF (Figure 3d), 7.5EPZF (Figure 3e) samples were 28.84 μm，15.98 μm, 8.63 μm, 5.24 μm and 3.17 μm. The change of coating roughness showed that the roughness of composite coating decreased obviously with the increase of epoxy resin content. When the amount of epoxy resin was 7.5 g, the 7.5EPZF

199 composite coating was almost flat which was consistent with the results observed in

200 Figure 1i and j.

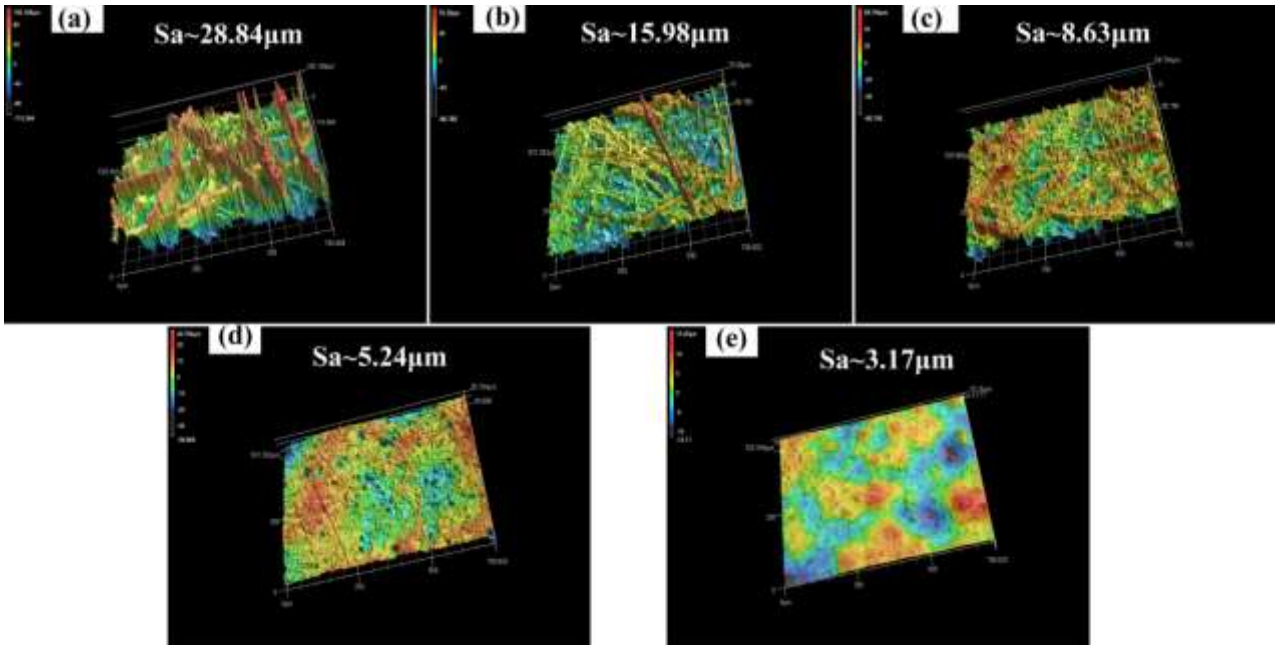

201

202 **Figure. 3.** The 3D morphology of the PZF (a) and 0.5PZF (b), 2.5EPZF (c), 5EPZF (d), 7.5EPZF (e) samples.

203 *3.3. Wetting behaviors*

204 The wettability of liquid droplets is an essential indicator to measure the protective

205 properties of the coating. The hydrophobic performance can significantly prevent

206 corrosive media and wetting, and prolong the service life of the coating. The contact

207 angle (CA) of the coated samples was tested by the contact angle tester (Dataphysics

208 OCA 15EC, Germany). The volume of the drops of deionized water was 5μl. The

209 5-point measurements were tested for each sample. The contact angle test results of

210 PZF, 0.5PZF, 2.5EPZF, 5EPZF, 7.5EPZF were shown in Figure 4.

In Figure 4a the contact angle test showed that the CA of the PZF composite coating was 143±1.3°. The PZF composite coating did not reach the superhydrophobicity (150°). As shown in Figure 1a and b, the reason was that the PZF coating was a loose porous structure and the excessive distance between the PZF silk made the hydrophobic air film discontinuous. With the increase of epoxy resin content, the contact angle began to increase. The CA of 0.5EPZF and 2.5EPZF composite coating were 152.2 ± 1.6° (Figure 4b) and 156.6 ± 1.5° (Figure 4c), respectively. And the SA of 2.5EPZF composite coating was < 10°. As the amount of epoxy resin continued to increase, the CA of the composite coating decreased. The CA of the 5EPZF composite coating and 7.5EPZF composite coating decreased to 151.3 ± 1.6° (Figure 4d) and 129.7 ± 2.1° (Figure 4e), respectively. It illustrated that the composite coating changed from superhydrophobic to hydrophobic.

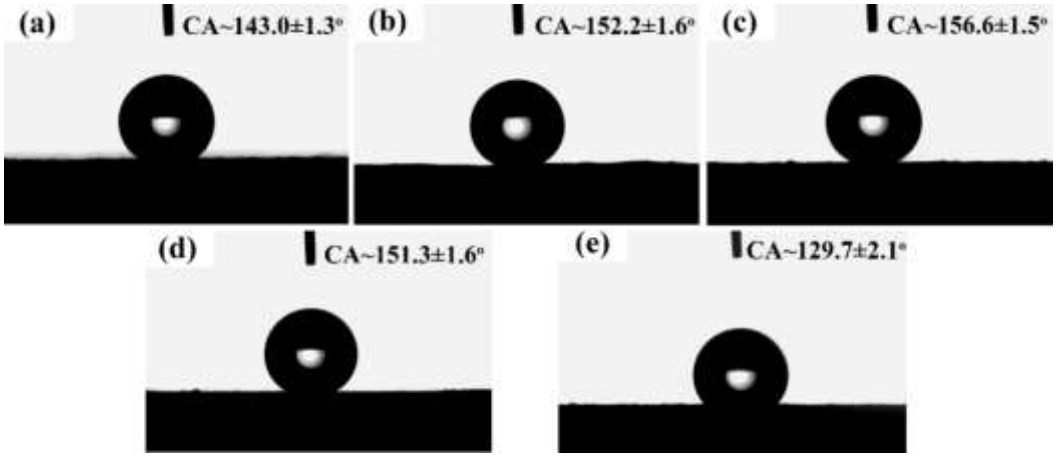

Figure. 4. The contact angle test results of PZF (a), 0.5EPZF (b), 2.5EPZF (c), 5EPZF (d) and 7.5EPZF (e) samples.

3.4. Formation mechanism for the composite coating

The formation mechanism for the composite PZF and EPZF was shown in Figure 5. Without EP, the mixture of PCL, ZnO and PFDTES could form into the filamentous interweaving after the mixture spraying from the spray gun nozzle. It was because the PCL was a long chain macromolecules polymer with fewer branched chains. As the solvent evaporates, the PCL of the mixture would exhibit a certain directional arrangement to form a filamentous structure (Figure 5a). The curing mechanism of epoxy resin was shown in Figure 5d. After curing, epoxy resin was a long-chain high polymer with a three-dimensional configuration and the network structure of EP partly restricted the directional arrangement of long chain molecules (PCL) [39,40].

Additionally, the crosslinking of EP improves significantly as the amount of EP reagent added increases. As the addition amount of EP gradually increased, the coarse branch structure duly became thicker and more numerous (Figure 5b). When the addition amount of EP was 2.5 g, the composite coating was with a certain number of 0.1-0.4 μm filamentous structure and a significant amount 1-3 μm coarse branch structure (Figure 1e and f, Figure 2c). Furtherore, with the addition amount of EP increased to 5 g and more, the crosslinking degree of epoxy resin continued to increase

and the filamentous structure&coarse branch structure vanished to form an overall block structure coating (Figure 5c). Figure 5e was the hydrolysis of PFDTES [46]. The hydrolysis product of PFDTES would combine with hydroxyl groups (ZnO and EP) to form a modified surface (Figure 5f) [47, 48]. On the other side, due to the hydrophilic group (-OH) of epoxy resin itself, when the amount of epoxy resin reached a certain level, the composite coating became hydrophilic from hydrophobic.

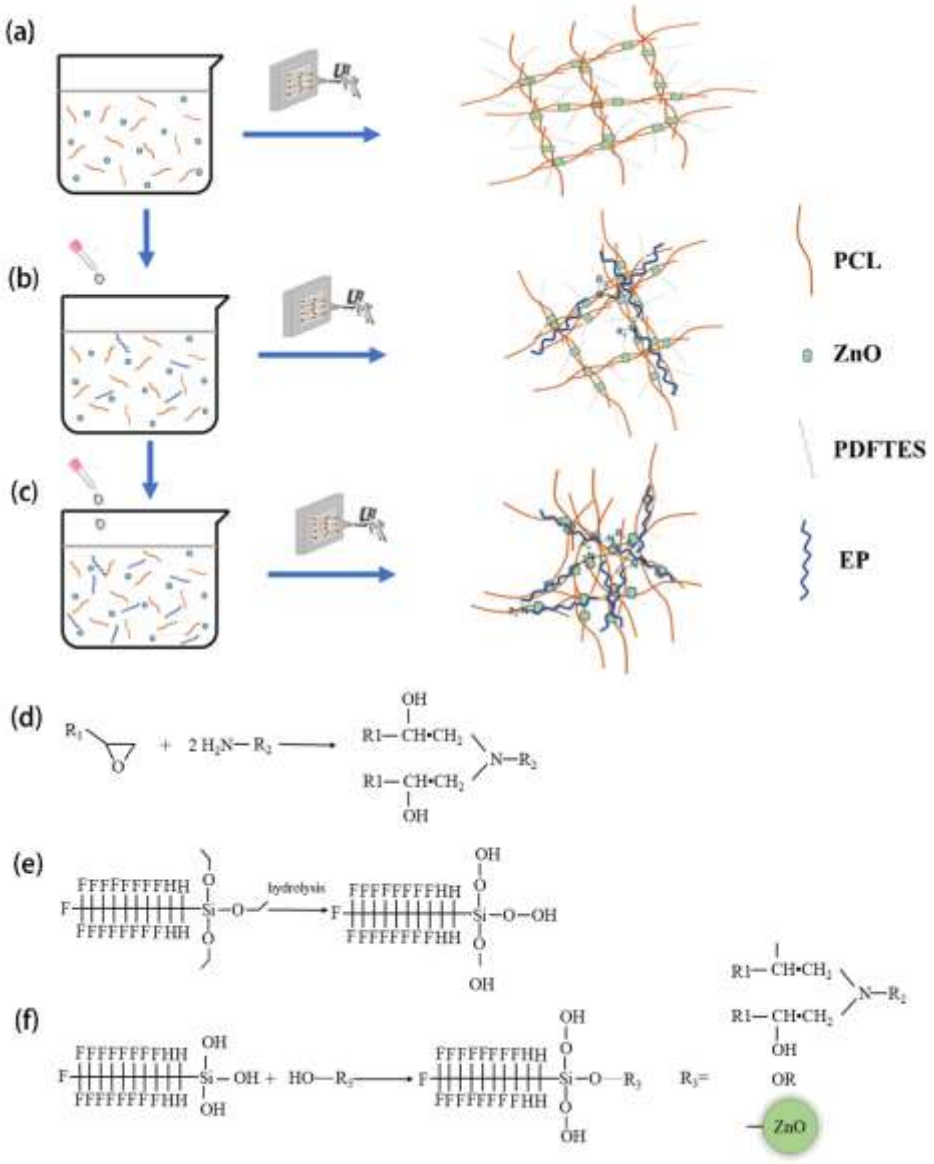

Figure. 5. Formation mechanism for the composite coating of PZF and EPZF composite coating.

3.5. Electrochemical corrosion behavior

With a three-electrode system in 300 mL 3.5 wt.% NaCl electrochemical impedance spectra (EIS) were carried out [49]. Samples were exposed with a surface area of 1 cm^2. A saturated calomel and a platinum mesh electrode were used as the reference and the counter electrode, respectively. At the open circuit potential (Ecorr), the scanning frequency range of electrochemical impedance test was 10^5-10^{-2} Hz, and the amplitude of sine wave disturbance was 10mV. The scanning rate of potentiodynamic polarization curve was 0.5 $mV \cdot s^{-1}$.

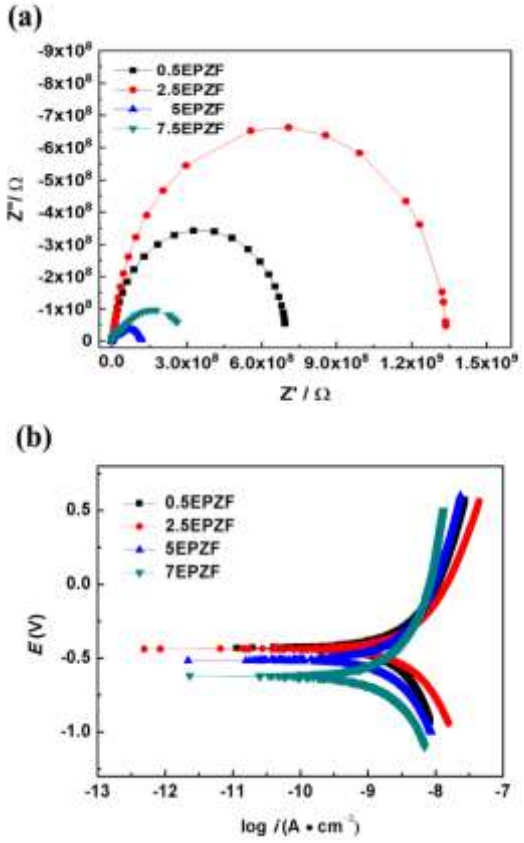

Figure. 6. EIS and potentiodynamic polarization results of EPZF composite coating with different amounts of epoxy resin.

Figure 6 showed the EIS (a) and potentiodynamic polarization test results (b) of the composite 0.5PZF, 2.5EPZF, 5EPZF, 7.5EPZF coating respectively. The size of impedance arc could objectively reflect the corrosion performance of the coating. The Nyquist diagram of EPZF composite coating with different amounts of epoxy resin was shown in Figure 6a. With the addition of epoxy resin, the impedance arc was the largest when the amount of epoxy resin is 2.5 g, about 1.37 x 10^9.

Samples	I_{cor} (A/cm^{-2})	E_o (V)	Corrosion Rate (mm/a)
0.5EPZF	6.2351 x 10^{-10}	-0.43216	7.6118 x 10^{-6}
2.5EPZF	1.043 x 10^{-12}	-0.43877	1.2733 x 10^{-8}
5EPZF	1.2716 x 10^{-8}	-0.7174	1.5524 x 10^{-4}
7.5EPZF	5.6863 x 10^{-9}	-0.6224	6.9419 x 10^{-5}

Table 2. E_{corr}, i_{corr} and Corrosion Rate of the EPZF composite coating on Mg substrate with different amounts of epoxy resin immersed in NaCl aqueous solutions (3.5 wt.%).

The electrochemical polarization test showed that with the increase of the amount of epoxy resin, the corrosion current of the coating first decreased from 6.2351 x 10^{-10} A•cm^{-2} (0.5EPZF) to 1.043 x 10^{-12} A•cm^{-2} (2.5EPZF) with the addition of epoxy resin from 0.5 g to 2.5 g. Then with the increase of epoxy resin content to 5.0 g, the corrosion current enhanced while the corrosion performance diluted. It was because with the raise of the amount of epoxy resin to 2.5 g, the network structure of the coating became dense visibly, the porosity decreased significantly, and the proportion of coarse branches increased. The dense pores tightly grasped the air to form a stable

278 air protection film, and this coating could reach the superhydrophobic state of 156.6 ±
279 1.5°, making the coating have good corrosion resistance. The thickness of 2.5EPZF
280 composite coating was only 77 μm. However, the 2.5EPZF composite coating had
281 relatively best corrosion protection performance. When the amount of epoxy resin
282 continued to increase to 5 g, the quality of porous structure was with a sharp decline.
283 The contact angle test also showed that the hydrophobic property of the 5EPZF coating
284 decreased demonstrably. The coating thickness of 5EPZF was 95 μm which was thicker
285 than 2.5EPZF, yet the corrosion rate of 5EPZF reduced by over 500 times. When epoxy
286 resin addition was 7.5 g, the porous structure of the 7.5EPZF coating almost
287 disappeared. At the same time, the 7.5EPZF coating was hydrophobic from
288 superhydrophobic. The coating thickness of 7.5EPZF reached 135 μm. It was about 1.6
289 times the thickness of 2.5EPZF coating, but its corrosion resistance was worse than
290 that of 2.5EPZF coating. It showed that the superhydrophobic three-dimensional
291 porous structure of the thinner composite coating could greatly enhance the corrosion
292 performance.

293 Here the 2.5EPZF sample was selected as the experiment sample, and magnesium
294 alloy and PZF coating sample was used as the controlled sample for the following

electrochemical performance and adhesion test of marine bacterium (Bacillus subtilis). Figure 7 showed the results of Nyquist impedance and potentiodynamic polarization tests of uncoated magnesium alloy samples, the PZF coating sample and the 2.5EPZF coating sample. EIS and potentiodynamic polarization results illustrated that the 2.5EPZF composite coating had the best corrosion resistance. And the corrosion current of 2.5EPZF sample was 1.043 x 10^{-12} A•cm^{-2}.

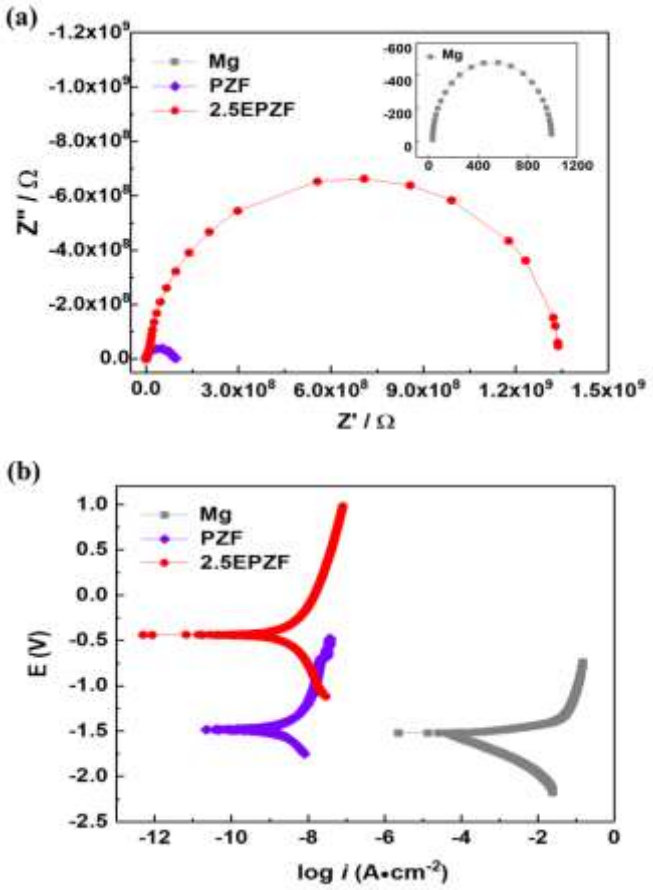

Figure. 7. The Nyquist diagramand and potentiodynamic polarization results of magnesium alloy substrate, PZF and 2.5EPZFsamples.

Samples	I_{cor} (A/cm^{-2})	E_o (V)	Corrosion Rate (mm/a)
Mg	6.4746 x 10^{-5}	-1.5532	1.3951
PZF	2.0373 x 10^{-11}	-1.0388	0.5239 x 10^{-7}

2.5EPZF	1.043 x 10^{-12}	-0.43877	1.2733 x 10^{-8}

Table 3. E_{corr}, i_{corr} and Corrosion Rate of the uncoated Mg substrate, PZF and 2.5EPZF composite coating immersed in NaCl Aqueous Solutions (3.5 wt.%).

Further, the EIS of the 2.5EPZF sample was tested in NaCl Aqueous Solutions (3.5 wt.%) after different immersion times for 0 day, 15 days, 25 days, 35 days at roomtemprature.

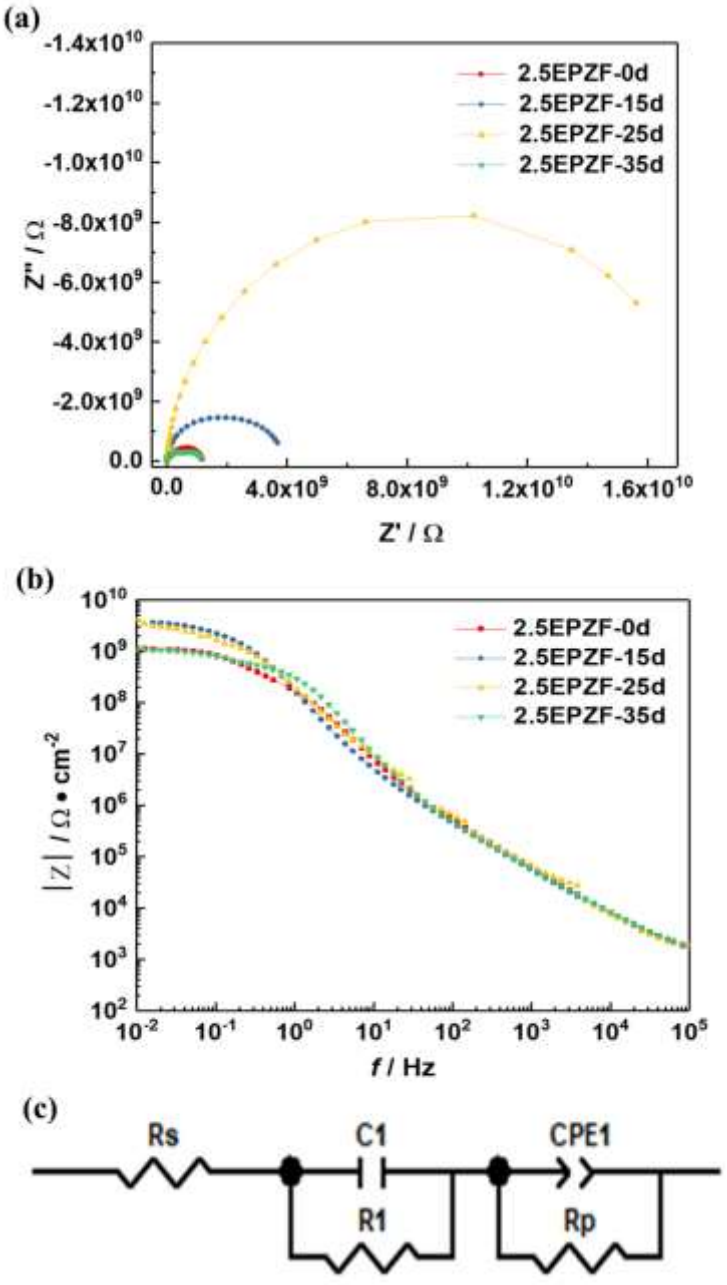

Figure. 8. Bode&Nyquist plots of 2.5EPZF composite coating at different immersion times in NaCl Aqueous Solutions (3.5 wt.%) and the corresponding equivalent electric circuit.

EIS of the 2.5EPZF sample in 3.5% NaCl solution for 35 days immersion was displayed in Figure 8. At the beginning, the Nyquist spectra present an arc with a large radius and the value of the low frequency impedance (|Z|0.01 Hz) in Bode spectra is about 1.37 x 10^9 Ω•cm^{-2}, manifesting high barrier property of the coating to the substrate [50]. As shown in the Nyquist diagram (Figure 8a), for the 2.5EPZF coating, the impedance modulus cut from 1.37 x 10^9 to 3.90 x 10^9 Ω•cm^{-2} severely after 15 days' immersion in NaCl Aqueous Solutions (3.5 wt.%). After 25 days' soaking, the impedance was increased to 1.60 x 10^{10} Ω•cm^{-2}. Under the pressure of the outside force (NaCl Aqueous Solutions), the deformation of treetop occurs and the pores of 2.5EPZF sample with mesh and skeleton coating become denser to grasp the air film firmly. It was caused by the diameter of mesh and skeleton of 2.5EPZF sample with about 0.1-0.4 μm Treetop structure and 1-3μm Branch structure. And the 1-3μm Branch structure of the 2.5EPZF coating provided the sufficient support to maintain the integrity of the air film. After 35 days' immersing, the impedance of 2.5EPZF sample was reduced to 1.30 x 10^8 Ω•cm^{-2}. During this time, the NaCl corrosion media gradually seeped into the surface of the air film with the measurably decrease of the

328 impedance modulus. Furthermore, the air film of 2.5EPZF coating was always present
329 during 35 days' immersion. After 35 days' immersion, the corrosion current of the
330 2.5EPZF coating was 1.1703 x 10^{-11} A•cm^{-2}.

331 Figure 8a, 8b displayed Nyquist and Bode plots of 2.5EPZF specimens after
332 different time's immersion in the NaCl solution (3.5 wt.%). The lowest impedance was
333 related to the 2.5EPZF-35d sample. Nyquist plots for all 2.5EPZF samples with
334 different time immersion consisted of two semi-circles. One semi-circle of the
335 composite coating was related to coating properties in the high-frequency range and
336 another one was attributed to double layers characteristics in the low-frequency range.

337 The Z view software was utilized for corresponding equivalent electrical circuits
338 (Figure 8c). The circuits had various elements such as solution resistance (Rs),
339 charge-transfer resistance (Rp), double layer constant phase element (CPEdl), pore
340 resistance (Rc), and coating constant phase element (CPEc). The highest value of
341 composite coating resistance was related to 2.5EPZF-25d sample (1003 Ωcm^2). The
342 lowest value of CPEp has also corresponded to 2.5EPZF-25d sample (3.008 x 10^{-10}).
343 After 35 days' immersion the impedance of 2.5EPZF-35d sample decreased to below
344 the impedance of 2.5EPZF-0d. It could be owed to the marvelous barrier property of

345 the superhydrophobic three-dimensional porous structure and after 35 days' immersion
346 the corrosive media was partially wetted the 2.5EPZF coating.

347 *3.6. Protection mechanism for 2.5EPZF composite coating*

348 Figure 9 was the schematic representation of the Load-bearing corrosion protection
349 mechanism for 2.5EPZF composite coating. The three-dimensional structure of
350 2.5EPZF composite coating was like the Branch and Treetop. As shown in Figure 1f,
351 the 0.1-0.4 μm mesh and 1-3 μm skeleton of 2.5EPZF sample played the role as the
352 Branch and Treetop of the tree, respectively. Under the pressure of the outside force
353 (pressure of the corrosive medium), the deformation of treetop occurs and the pores of
354 mesh and skeleton coating become denser to grasp the air film firmly. Furthermore, the
355 1-3 μm Branch structure of the 2.5EPZF coating provided the sufficient support to
356 maintain the integrity of the air film. Then the Load-bearing type 2.5EPZF composite
357 coating could afford more durable protection from corrosive media in the case of
358 thinner coating.

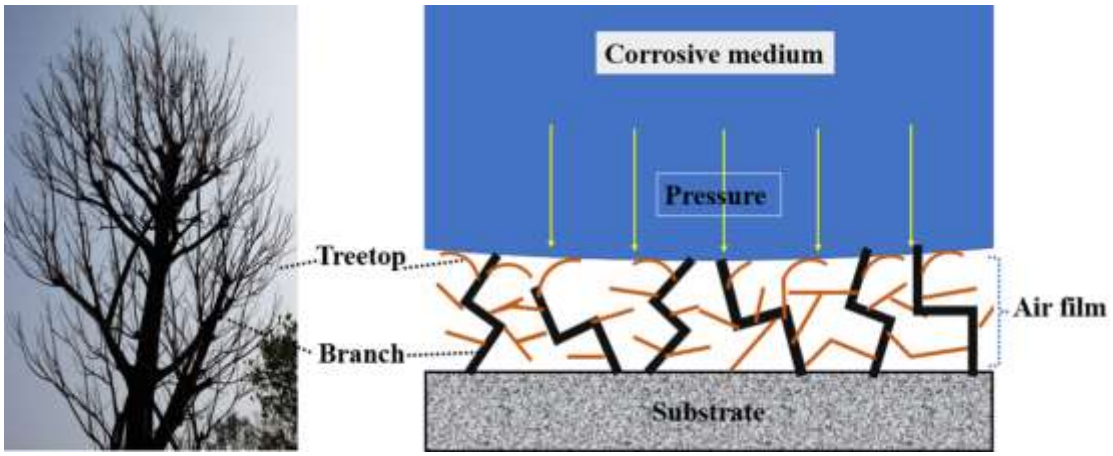

Figure. 9. Schematic representation of the Load-bearing type corrosion protection mechanism for 2.5EPZF composite coating.

3.7. FT-IR spectra of PCL, PZ, PZF and 2.5EPZF coating&mechanical adhesion and self-cleaning tests

The FT-IR spectra of PCL, PZ, PZF and 2.5EPZF coating&mechanical adhesion and self-cleaning tests were shown in Figure 10. The specific functional groups for PCL, PZ, PZF and 2.5EPZF coating were evaluated by FTIR absorbance as shown in Figure 10a. The bands observed at 2960-2870 cm^{-1} and 1725 cm^{-1} were related to tensile vibrations of C-H and Stretching vibrations of the ester carbonyl group, respectively [51, 52]. Furthermore, bands at 1462 cm^{-1} and 1066 cm^{-1} were related to C-C and C-H tension [46]. It was determined that the perceptible signal at 400-600 cm^{-1} increased with the addition of ZnO. The reason was that the ZnO material had an intense IR band centered at 442 cm^{-1} in the spectral region 0-600 cm^{-1} [53]. The absorption bands appearing at 1300 cm^{-1} - 1000 cm^{-1} was attributed to the stretching mode of CF_2 [54].

374 With the addition of PDFTES, the peaks between 1300 cm^{-1} - 1000 cm^{-1} increased.
375 During solidification of the coating, EP and its cross-linker formed a net, and the
376 PDFTES would move towards the surface during the coat's solidification because the
377 PFDTES was highly hydrophobic and the EP system was hydrophilic [46]. The
378 characteristic absorption peaks of Si-O and O-Si-O appeared at 1035 cm^{-1} and 827 cm^{-1},
379 which illustrated that the amount of PFDTES on the surface of 2.5EPZF sample
380 significantly increased [55]. It indicated that PFDTES had transferred to the surface of
381 the composite coating with solidification of EP.

382 Generally, the stability of adhesive materials on the surface is one of the main
383 challenges of coating [56,57]. The adhesion strength between coating and magnesium
384 alloy was evaluated according to ASTM D3359-09 method [49]. The result of adhesion
385 measurement illustrated that the 2.5EPZF coating in Figure 10b showed very few
386 flakes detached at intersections. It suggested that the bonding strength between the
387 2.5EPZF coating and magnesium sample was strong enough to be potentially used in
388 physiological environments.

389 Lotus-inspired superhydrophobic surface features self-cleaning effect [58]. The
390 self-cleaning ability of 2.5EPZF coating was evaluated and displayed in Figure 10c.

Due to the SA being less than 10°, water droplets could slide on the surface of the 2.5EPZF sample easily. And the self-cleaning test was measured to evaluate the self-cleaning ability of the 2.5EPZF coating as shown in Figure 10c. The self-cleaning test result illustrated that the sand on the surface of the 2.5EPZF sample was carried away mostly after 10 water droplets, which proved that the composite coating was with good self-cleaning performance.

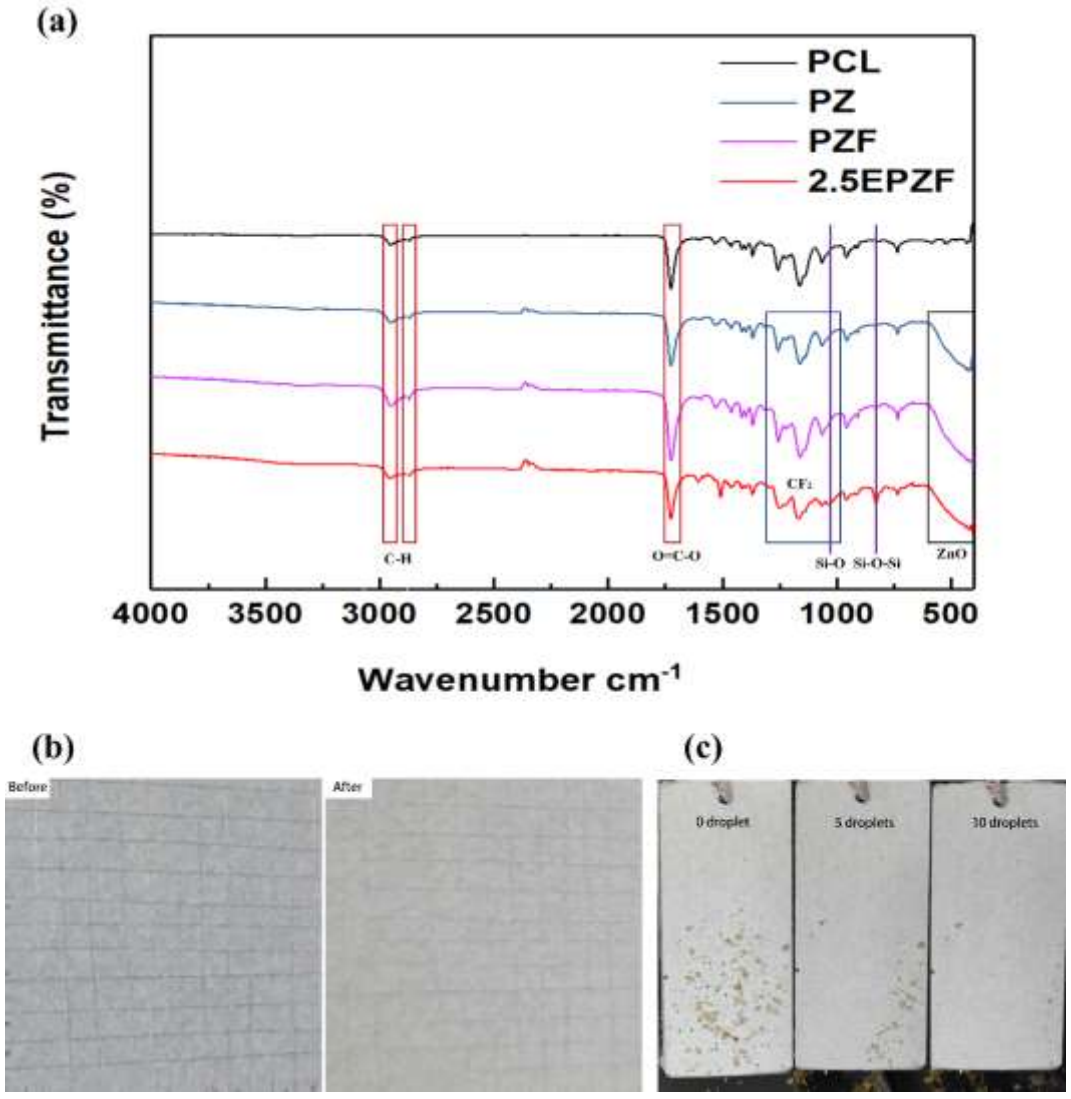

Figure. 10. FTIR analysis of PCL, PZ, PZF and 2.5EPZF coating (a), the results of mechanical adhesion (b) and self-cleaning test (c).

3.8. Abrasion resistance and pH stability test

Figure 11 showed the results of abrasion resistance test and pH durability of 2.5EPZF coating. The mechanical abrasion resistance of 2.5EPZF was measured by the sandpaper abrasion test to evaluate the tribological properties [59, 60]. The result of the 2.5EPZF coating's sandpaper abrasion experiment was as shown in Figure 11a. The 2.5EPZF coating was abraded on a 1000-mesh sandpaper under a weight of 360.0 g at a constant speed of 1 cm/s. After 3 cycles of total length of 30 cm, the CA of 2.5EPZF coating was 151.1 ± 1.2° with a small amount of debris falling.

The contact angle test of the water droplets with different pH values was carried out on the surface of the 2.5EPZF coating to determine the resistance of the coating to acid and alkali solutions. As shown in Figure 9b, the CA of the 2.5EPZF coating surface increased first and then decreased with the increase of pH value, but it is higher than 153°. The results indicated that the 2.5EPZF coating had excellent chemical stability.

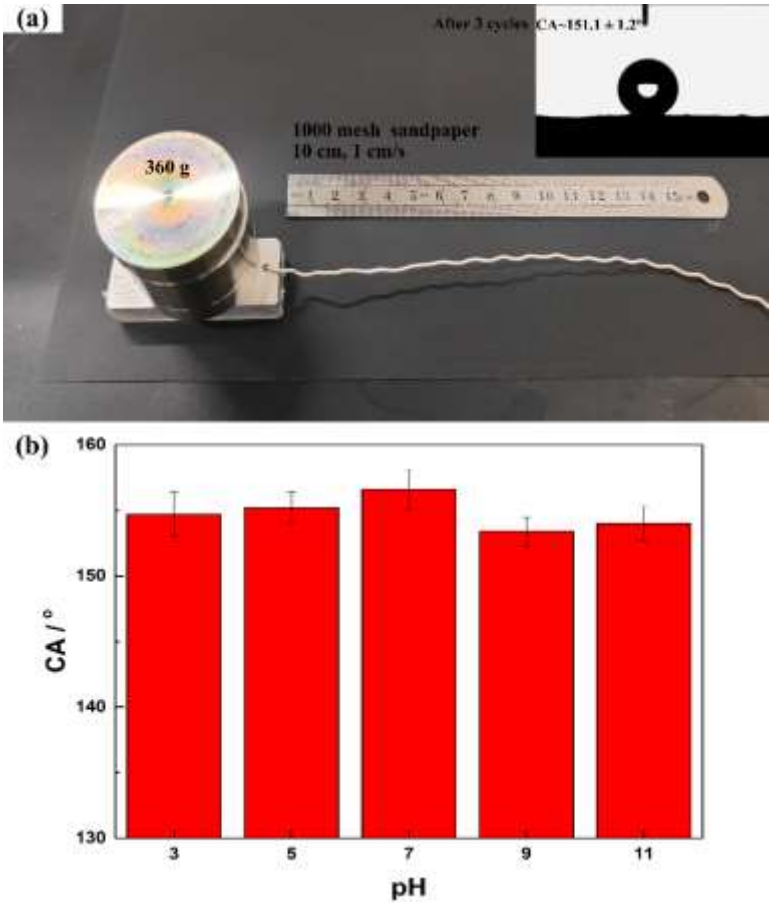

Figure. 11. The mechanical abrasion resistance (a) and pH durability (b) of 2.5EPZF coating.

3.9. Bacillus subtilis adhesion test and corrosion resistance test

Figure 12 showed the results of Bacillus subtilis adhesion test for 20 days at 30 ºC and 120 prm and corrosion resistance test in 3.5% wt NaCl at room temperature. In experiment, three parallel samples from each group. After the bacterial adhesion test, the tested samples were fixed in 2.5% glutaraldehyde aqueous solutions for 20 minutes. Then divided them into ethanol solution at 5%, 15%, 25%, 45%, 65%, 85%, 95% of the step concentration in proper order. In the end, dehydrated in anhydrous ethanol for 20 minutes and dried for natural air. Figure 12a, b and c showed the digital photos and

SEM images of magnesium alloy substrate, PZF and 2.5EPZF samples after 20 days in Bacillus culture. Figure 12a, 12b and 12c were the digital photos and SEM images of magnesium alloy substrate, PZF and 2.5EPZF samples after the Bacillus subtilis adhesion test. There was the serious corrosion of the AZ91D magnesium alloy substrate as the Digital photo shown. Furthermore, there were many bacilli on the corrosion surface of magnesium alloy as shown in SEM image of Figure 12a. It showed that AZ91D magnesium alloy was prone to corrosion and microbial attachment in the marine environment containing Cl^- and marine bacteria (Bacillus). There were the perceptible coating damage and measurably bacillus adhesion of the magnesium substrate in the Bacillus environment for 20 days' immersion in Figure 10a. Compared with the magnesium alloy substrate, the PZF coating was damaged partially and the pitting pits were produced. It showed that the degradable PCL combined with PFDTES could not provide sufficient protection for magnesium alloy in the marine environment containing Cl^- and marine bacteria (Bacillus). In Figure 12b, the SEM image of some residual PZF coating illustrated that the PZF coating had a good anti-adhesion effect against Bacillus. Figure 12c was the digital photo and SEM image of the 2.5EPZF composite coating sample after 20 days' immersion in the Bacillus environment. The

results showed that the 2.5EPZF composite coating had no obvious surface damage and corrosion. The protective 2.5EPZF coating was still intact and the three-dimensional structure of the coating was also maintained. What's more, there was no obvious bacillus adhesion. It showed that 2.5EPZF composite coating could provide sufficient protection for magnesium alloy samples and had strong adhesion resistance to marine bacteria Bacillus.

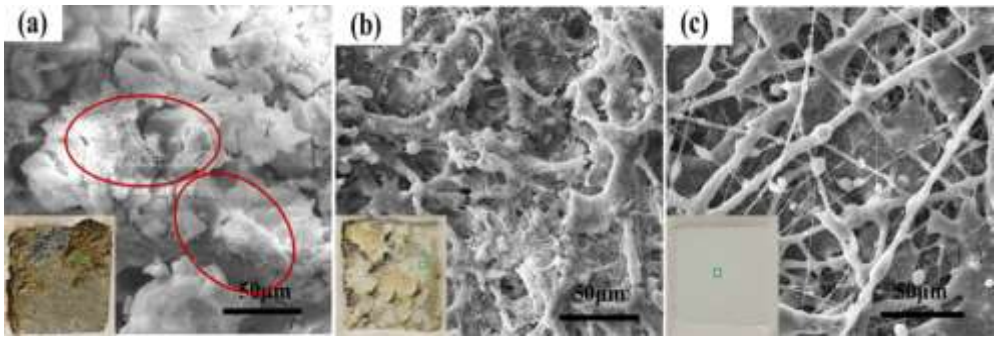

Figure. 12. Digital photos&SEM images of magnesium alloy substrate (a), PZF (b) and 2.5EPZF (c) samples after 20 days in Bacillus culture at 30°C: magnesium alloy substrate.

3.10. Solar irradiation and thermal repair, grid corrosion test

Drew a big cross on the surface of superhydrophobic 2.5EPZF composite coating with a surgical blade. The scratch depth exposed the magnesium alloy, and the scratch width was about 20-25 μm. A group of crossed 2.5EPZF composite coating samples were exposed to outdoor direct sunsolar irradiation for 6 hours (Wuhan, September). Another group of crossed 2.5EPZF composite coating was placed in an oven at 50 °C for 30 min, and then took out to the air and cooled to room temperature. The crossed

456 2.5EPZF samples without solar irradiation or heating were used as the control group.
457 During the accelerated corrosion test of scratched 2.5EPZF samples, the above three
458 groups of samples were placed in the 10% wt NaCl solutions at 30 °C for 24 hours.
459 After that, took them out to the outdoor environment for 20 days to observe the surface
460 changes of the samples (as shown in Figure 13). The 2.5EPZF samples before (Figure
461 13a) and after (Figure 13d) grid corrosion test and the SEM image (Figure 13g)
462 illustrated that the 2.5 EPZF composite coating could provide protection for
463 magnesium alloy matrix, and only corrosive medium infiltration occurs at the scratch.
464 The 2.5EPZF samples under 6 hours' solar irradiation before (Figure 13b), after
465 (Figure 13e) grid corrosion test and the 2.5EPZF samples at 50 °C for 30min before
466 (Figure 13c), after (Figure 13f) grid corrosion test showed that there was no corrosive
467 medium infiltration at the scratch. It showed that 2.5EPZF sample would be repaired to
468 a certain extent after sunsolar irradiation or at 50 °C for 30 min to prevent the
469 corrosion damage of corrosion medium NaCl to the sample.
470 The EDS data (Table 4) showed that the content of Si and F of 2.5EPZF coating
471 increased significantly after illumination and heating at 50 °C. Under the solar
472 irradiation or heating at 50 °C, the PFDTES on the coating surface would undergo a

certain amount of molecular transfer and the redistribution of perfluorinated branched chains, which would repair the scratch gap to a certain extent, increase the hydrophobicity, reduce the invasion of corrosive media, and improve the corrosion protection ability of scratches.

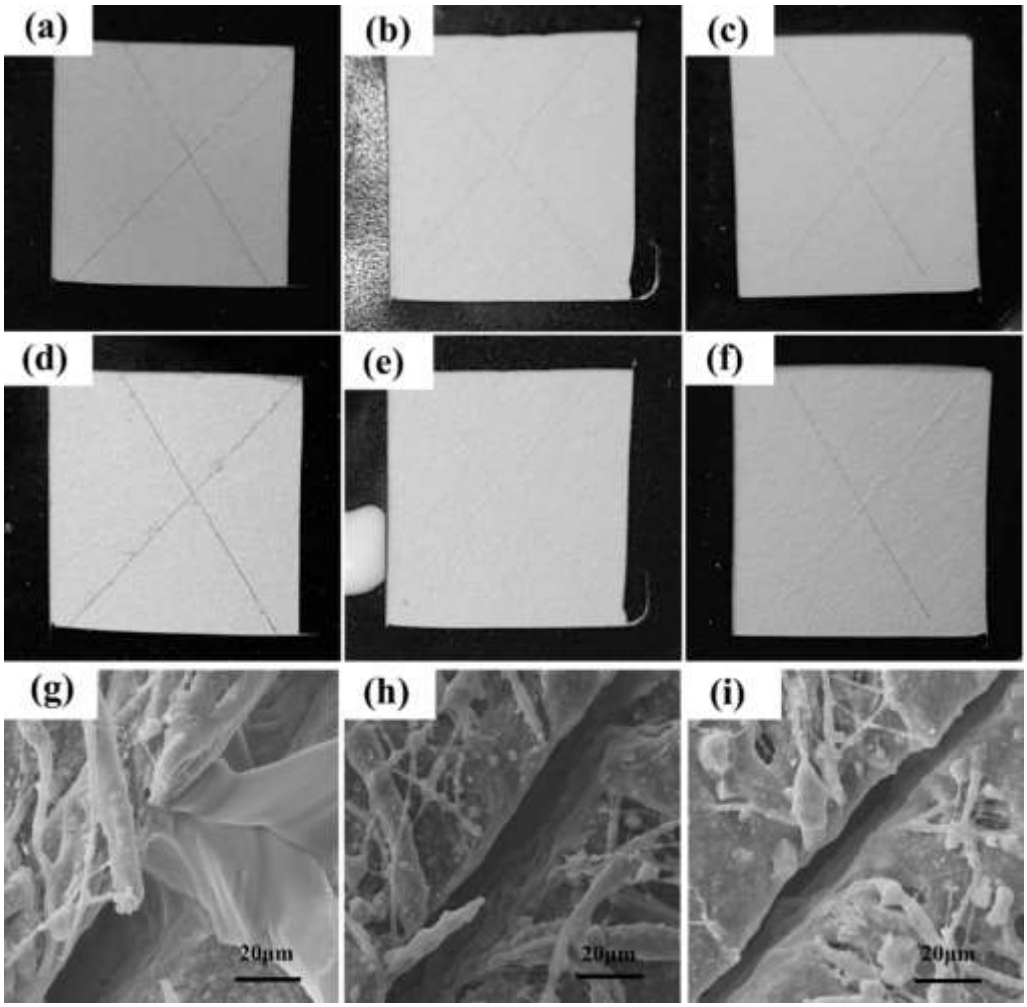

Figure. 13. Digital photos scratched 2.5EPZF samples before&after grid corrosion test, 2.5EPZF samples at 50 °C for 30 min before (c)&after (f) grid corrosion test and the SEM of sample of scratched 2.5EPZF after accelerated corrosion test; 2.5EPZF samples before (a)&after (d) grid corrosion test； 2.5EPZF samples under solar irradiation before (b) and after (e) grid corrosion test; 2.5EPZF samples at 50 °C for 30 min before (c) and after (f) grid corrosion test and the SEM of sample of scratched 2.5EPZF after accelerated corrosion test; 2.5EPZF samples under solar irradiation before (b) and after (e) grid corrosion test; 2.5EPZF samples at 50 °C for 30 min before (c) and after (f) grid corrosion test.

Samples	C/ wt%	O/ wt%	Zn/ wt%	F/ wt%	Si/ wt%

2.5EPZF	60.0	18.6	16.7	4.4	0.3
2.5EPZF after sunsolar irradiation	54.6	22.3	17.9	4.8	0.4
2.5EPZF at 50°C for 30min	55.0	21.9	17.4	5.2	0.5

485 **Table 4.** The EDS of samples with 2.5EPZF composite coating.

486 *3.11. The large scale&irregular shape preparation of 2.5EPZF coating and their*

487 *superhydrophobicity*

488 The preparation of the large scale&irregular shape with the superhydrophobic

489 2.5EPZF coating was shown in Figure 14. In Figure 14a, the results illustrated that the

490 spraying method to prepare the 2.5EPZF coating could complete the large area

491 preparation and the composite 2.5EPZF coating was with the superhydrophobicity of

492 ink, juice, milk and tea. Figure 14b indicated that the preparation of superhydrophobic

493 coating could be assisted in rapid application to irregularly shaped substrate.

494

495 **Figure. 14.** Digital photos of the large scale&irregular shape samples with 2.5EPZF coating and their

496 superhydrophobicity: (a) large scale samples with 2.5EPZF coating and the superhydrophobicity of ink, juice,

497 milk and tea; (b) irregular shape samples with 2.5EPZF coating and the superhydrophobicity of water 2.5EPZF

498 samples.

499 **4. Conclusions**

In this study, by one-step spray method a three-dimensional superhydrophobic 2.5EPZF composite coating was prepared. The spraying method provides a feasible solution to prepare the controllable three-dimensional structure coating. The 2.5EPZF composite coating has durable hydrophobic, good mechanical adhesion and self-cleaning, antifouling and corrosion resistance. The composite coating also has the function of repairing scratches under sunsolar irradiation and heating at 50 ºC. Furthermore, the superhydrophobic large scale&irregular shape of 2.5EPZF composite coating can be prepared. The above functions have application value for the application of 2.5EPZF composite coating in marine ships.

Declaration of Competing Interest

The authors declare that they have no known competing financial interests or personal relationships that could have appeared to influence the work reported in this paper.

Acknowledgment

We gratefully acknowledge financial support from the Innovation and Development Joint Fund Key Project of Hubei Provincial Natural Science Foundation (2022CFD029).

References

[1] M.S. Joun, S.M. Ji, J.D. Yoo, S.H. Chung, H.K. Moon, E.J. Kim, D.J. Yoon, J.M. Choi, A. Babu, Characterization of AZ31B, AZ61A and AZ80A magnesium alloys with an emphasis on temperature compensation for their application to a hot forging. J. Manuf. Process. 84 (2022) 764-785, https://doi.org/10.1016/j.jmapro.2022.10.054.

[2] X.D. Chen, Q.Z. Cai, Z.W. Deng, L.S. Yin, Research and Application of Micro-Arc Oxidation Technology on Magnesium Alloy Motorcycle Key Parts. Appl. Mechan. Mater. 496-500 (2014) 63-70, https://doi.org/10.4028/www.scientific.net/amm.496-500.63.

[3] S. Chen, J. Zhang, Y. Chen, S. Zhao, M. Chen, X. Li, F.M Manfred, J. Wang, N. Huang, Application Of Phenol/Amine Copolymerized Film Modified Magnesium Alloys: Anticorrosion And Surface Biofunctionalization. ACS Appl. Mater. Interfaces. 7 (2015) 24510-24522, https://doi.org/10.1021/acsami.5b05851.

[4] G. Wang, J.P. Weiler, Recent developments in high-pressure die-cast magnesium alloys for automotive and future applications, J. Magnes. Alloy. 11 (2023) 78-87.

[5] J. Moreno, J.L. Merlo, A.C. Renno, J. Canizo, F.J. Buchelly, J.I. Pastore, M.R. Katunar, S. Cere, In vitro characterization of anodized magnesium alloy as a potential biodegradable material for biomedical applications, Electrochim. Acta. 437 (2023) 141463, https://doi.org/10.1016/j.electacta.2022.141463.

[6] M. Ahmadi, S.A.A.B Tabary, D. Rahmatabadi, M.S. Ebrahimi, K. Abrinia, R. Hashemi, Review of selective laser melting of magnesium alloys: advantages, microstructure and mechanical characterizations, defects, challenges, and applications, J. Mater. Re. Technol. 19 (2022) 1537-1562, https://doi.org/10.1016/j.jmrt.2022.05.102.

[7] P. Karuppusamy, K. Lingadurai, V. Sivananth, S. Arulkumar, A study on mechanical properties of tungsten carbide reinforced magnesium metal matrix composites for the application of piston, Int. J. Solar irradiationweight Mater. Manuf. 4 (2021) 449-459, https://doi.org/10.1016/j.ijlmm.2021.06.007.

[8] J.M. Seitz, R. Eifler, M. Vaughan, C. Seal, M. Hyland, H.J. Maier, Coating Systems for Biodegradable Magnesium Applications, Magnes. Technol. 2014, pp. 371-374.

[9] H. Hu, A. Yu, N. Li, J.E. Allison, Potential Magnesium Alloys for High Temperature Die Cast Automotive Applications: A Review. Mater. Manuf. Process. 18 (2003) 687-717, https://doi.org/10.1081/AMP-120024970.

[10] A.M. Zhang, P. Lenin, R.C. Zeng, M.B. Kannan, Advances in hydroxyapatite coatings on biodegradable magnesium and its alloys, J. Magnes. Alloy. 10 (2022) 1154-1170, https://doi.org/10.1016/j.jma.2022.01.001.

[11] X. He, J. Liu, C. Yang, G. Jiang, Predicting thermodynamic stability of magnesium alloys in machine learning, Comp. Mater. Sci. 223 (2023) 112111, https://doi.org/10.1016/j.commatsci.2023.112111.
[12] J. Jiang, Y. Wang, Y. Li, W. Shan, S. Luo, Microstructure and mechanical properties of the motorcycle cylinder body of AM60B magnesium alloy formed by combining die casting and forging, Mater. Design. 37 (2012) 202-210, https://doi.org/10.1016/j.matdes.2012.01.012.
[13] Y.K. Gao, D.W. Gao, Y.H. Gao, A Study on Magnesium Alloy Substitution Design and Analysis for Automotive Seat Back Frame, Adv. Mater. Res. 156-157 (2010) 245-251, https://doi.org/10.4028/www.scientific.net/AMR.156-157.245.
[14] A. Kiełbus，T. Rzychoń，R. Cibis, Microstructure of AM50 die casting magnesium alloy. J. Achiev. Mater. Manuf. Eng. 18 (2006) 135-138.
[15] H. Friedrich, S. Schumann, Research for a “new age of magnesium” in the automotive industry, J. Mater. Proc. Technol. 117 (2001) 276-281, https://doi.org/10.1016/S0924-0136(01)00780-4.
[16] C. Suman, The Effects of Direct Aging on Mechanical Properties and Corrosion Resistance of Diecast Magnesium Alloys AZ91D and AM60BN, SAE Technical Paper 900794, SAE February-March, l990.
[17] A. Kieábus, M. SozaĚska, L. Cizek, Microstructural characterization of AZ91 magnesium alloy, Magnesium Alloys and Their Applications, Wolfsburg. 2003. pp. 190-195.
[18] X. Jia, J. Song, B. Xiao, Q. Liu, H. Zhao, Z. Yang, J Liao, L. Wu, B. Jiang, A. Atrens, F. Pan, Influence of indentation size on the corrosion behaviour of a phosphate conversion coated AZ80 magnesium alloy, J. Mater. Res. Technol. 14 (2021) 1739-1753, https://doi.org/10.1016/j.jmrt.2021.07.091.
[19] J. Ouyang, Y. Gao, Dense nanoarrays LDHs film evenly dividing the Cl^- diffusion path into longitudinal microchannels in favor of quasi-uniform corrosion of biomedical magnesium alloys，Surf. Coat. Tech. 449 (2022) 128981, https://doi.org/10.1016/j.surfcoat.2022.128981.
[20] F. Ge, Z. Cui, Y. Liu, L. Lei, X. Wang, H. Cui, Influence of ammonium sulfate on the corrosion behavior of AZ31 magnesium alloy in chloride environment, J. Magnes. Alloy. xxx (xxxx) xxx, https://doi.org/10.1016/j.jma.2022.07.014.
[21] B. Vaghefinazari, S.V. Lamaka, C. Blawert, M. Serdechnova, N. Scharnagl, P. Karlova, D.C.F. Wieland, M.L. Zheludkevich, Exploring the corrosion inhibition mechanism of 8-hydroxyquinoline for a PEO-coated magnesium alloy. Corros. Sci. 203 (2022) 110344, https://doi.org/10.1016/j.corsci.2022.110344.
[22] S.M. Ganji, M. Tehranchi, A. Ehterami, H. Semyari, F. Taleghani, M. Habibzadeh, M.H. Tayeed, N. Mehrnia, A. Karimi, M. Salehi, Bone tissue engineering via application of a

585 PCL/Gelatin/Nanoclay/Hesperetin 3D nanocomposite scaffold, J. Drug Deliv. Sci. Tec. 76 (2022)
586 103704, https://doi.org/10.1016/j.jddst.2022.103704.
587 [23] Q.Z. Yuan, C. Shi, T.S. He, Design and performance optimization of self-cleaning coating on
588 decorative UHPC surface, Constr. Build. Mater. 394 (2023) 132115,
589 https://doi.org/10.1016/j.conbuildmat.2023.132115.
590 [24] J. Lv, C.X. Zhu, H.N. Qiu, J. Zhang, C.D. Gu, J. Feng, Robust icephobic epoxy coating using
591 maleic anhydride as a crosslinking agent, Prog. Org. Coat. 142 (2020) 105,
592 https://doi.org/10.1016/j.porgcoat.2020.105561.
593 [25] X.Q. Fan, S.J. Song, Y.T. Shi, M. Cai, Y. Huang, B.B. Zhang, M.H. Zhu, Mechanochemical
594 stable superhydrophobic coating toward lasting corrosion protection, Prog. Org. Coat. 178 (2023)
595 107478, https://doi.org/10.1016/j.porgcoat.2023.107478.
596 [26] Z.X. Yang, L.C. Jing, X.B. Ming, W.H. Geng, W.W. Cao, Y.H. Tian, P.S. Bin, Z.L. Bao, R.Y.
597 Chang, H.Z. Geng, Preparation and performance study of superhydrophobic layer based on fluffy
598 ZnO rods/PDMS, Surf. Interfaces. 39 (2023) 102968,
599 https://doi.org/10.1016/j.surfin.2023.102968.
600 [27] G.H. Zhang, P.P. Wang, X.X. Zhang, C.H. Xiang, L.L. Li, The preparation of PCL/MSO/SiO_2
601 hierarchical superhydrophobic mats for oil-water separation by one-step method, Euro. Polym. J.
602 116 (2019) 386-3, https://doi.org/10.1016/j.eurpolymj.2019.04.011.
603 [28] Z.M. Jiang, B.T. D. Nguyen, J.H. Seo, C. Hong, D. Kim, S. Ryu, S. Lee, G. Lee, Y. H. Cho,
604 J.F. Kim, K. Lee, Superhydrophobic polydimethylsiloxane dip-coated polycaprolactone
605 electrospun membrane for extracorporeal membrane oxygenation, J. Membrane. Sci. 679 (2023)
606 121715, https://doi.org/10.1016/j.memsci.2023.121715.
607 [29] P. Cao, H. Wang, L.M. Zhao, Y.R. Zhou, J. Zhang, Y.Y. Zhang, L.X. Zheng, Q.W. Li, Robust,
608 amphiphobic and super-buoyant CNT foams promising for self-floating functional platforms,
609 Carbon. 168 (2020)439-447, https://doi.org/10.1016/j.carbon.2020.06.037.
610 [30] X.B. Zhang, Y.P. Hu, W. Yang, M.B. Feng, Ag-loaded and Pd-loaded ZnO nanofiber
611 membranes: preparation via electrospinning and application in photocatalytic antibacterial and
612 dye degradation, Appl. Nanosci. 13 (2023) 1495-1506,
613 https://doi.org/10.1007/s13204-021-02056-3.
614 [31] D.F. Arisoy, W.K. Kolewe, B. Homyak, S.I. Kurtz, D.J. Schiffman, J.J. Watkins, Bioinspired
615 Photocatalytic Shark-Skin Surfaces with Antibacterial and Antifouling Activity via Nanoimprint
616 Lithography. ACS Appl. Mater. Inter. 23(2018)20055-20063,
617 https://doi.org/10.1021/acsami.8b05066.

[32] S.D. Zhi, G. Wang, Z.X. Zeng, L.J. Zhu, Z.X. Liu, D.W. Zhang, K.L. Xu, Q.J. Xue, 3D mossy structures of zinc filaments: A facile strategy for superamphiphobic surface design, J. Colloid Interf. Sci. 526 (2018) 106-113, https://doi.org/10.1016/j.jcis.2018.04.083.

[33] K.M. Lee, H. Park, J. Kim, D.M. Chun, Fabrication of a superhydrophobic surface using a fused deposition modeling (FDM) 3D printer with poly lactic acid (PLA) filament and dip coating with silica nanoparticles, Appl. Surf. Sci. 467-468 (2019) 979-991, https://doi.org/10.1016/j.apsusc.2018.10.205.

[34] M. Amin, M. Singh, K.R. Ravi, Fabrication of superhydrophobic PLA surfaces by tailoring FDM 3D Printing and chemical etching process, Appl. Surf. Sci. (2023) 157217, https://doi.org/10.1016/j.apsusc.2023.157217.

[35] S. Rathinavel, P.S. Korrapati, P. Kalaiselvi, S. Dharmalingam. Mesoporous silica incorporated PCL/Curcumin nanofiber for wound healing application, Eur. J. Pharm. Sci. 167 (2021) 106021, https://doi.org/10.1016/j.ejps.2021.106021.

[36] J. Hu, B. Yang, F. Jin, P. Soo-Jin, Fracture toughness and surface morphology of polysulfone-modified epoxy resin. J. Ind. Eng. Chem. 25 (2015) 9-11, https://doi.org/10.1016/j.jiec.2014.10.032.

[37] M.Y. Li, Z.H. Min, Q.C. Wang, W. Huang, Z.Y. Shi, Effect of epoxy resin content and conversion rate on the compatibility and component distribution of epoxy asphalt: A MD simulation study, Constr. Build. Mater. 319 (2022) 126050, https://doi.org/10.1016/j.conbuildmat.2021.126050.

[38] F. Ferdosian, Y.S. Zhang, Z.S. Yuan, M. Anderson, C. Xu, Curing kinetics and mechanical properties of bio-based epoxy composites comprising lignin-based epoxy resins, Eur. Polym. J. 82 (2016) 153-165, https://doi.org/10.1016/j.eurpolymj.2016.07.014.

[39] S.R. Ravi, J.P. Girish, B. Vivek, I.K. Muhammad, E. Noureddine, S. Abdallah, L. Rafael，An eco-friendly approach on green synthesis, bio-engineering applications, and future outlook of ZnO nanomaterial: A critical review，Environ. Res. 221 (2023) 114807, https://doi.org/10.1016/j.envres.2022.114807.

[40] B. Baro, S. Khimhun, U. Das, S. Bayan, ZnO based triboelectric nanogenerator on textile platform for wearable sweat sensing application, Nano Energy. 108 (2023) 108212, https://doi.org/10.1016/j.nanoen.2023.108212.

[41] Y.L. Zhang, Y.L. Zhang, Y. Lei, J.R. Wu, Y.Y. Kang, S. Zheng, L.Q. Shao, MDM2 upregulation induces mitophagy deficiency via Mic60 ubiquitination in fetal microglial inflammation and consequently neuronal DNA damage caused by exposure to ZnO-NPs during pregnancy, J. Hazard. Mater. (2023) 131750, https://doi.org/10.1016/j.jhazmat.2023.131750.

652 [42] Y.J. Zheng, K.L. Wang, L. Sun, H.L. Shi, X. Zhang, Preparation of PFDTS-kaolin/PU
653 superamphiphobic coatings with antibacterial, antifouling and improved durability property, Prog.
654 Org. Coat. 173 (2022) 107145, https://doi.org/10.1016/j.porgcoat.2022.107145.
655 [43] P. Cao, H. Wang, L.M. Zhao, Y.R. Zhou, J. Zhang, Y.Y. Zhang, L.X. Zheng, Q.W. Li, Robust,
656 amphiphobic and super-buoyant CNT foams promising for self-floating functional platforms,
657 Carbon. 168 (2020)439-447, https://doi.org/10.1016/j.carbon.2020.06.037.
658 [44] B. Saha, W.Q. Toh, E. Liu, S.B. Tor, J. Lee, A study on frictional behavior of PMMA against
659 FDTS coated silicon as a function of load, velocity and temperature, Tribol. Int. 102 (2016) 44-51,
660 https://doi.org/10.1016/j.triboint.2016.04.018.
661 [45] P.Z. Wang, L. Zhang, Z.Q. Hu, J.Q. Shang, J. Zhou, Transparent and anti-fingerprint coating
662 prepared with chitin nanofibers and surface modification via vapor deposition, Prog. Org. Coat.
663 172 (2022) 107126, https://doi.org/10.1016/j.porgcoat.2022.107126.
664 [46] J. Zhang, W.C. Zhang, J.J. Lu, C.X. Zhu, W.Q. Lin, J. Feng, Aqueous epoxy-based
665 superhydrophobic coatings: Fabrication and stability in water, Prog. Org. Coat. 121 (2018) 201-2,
666 https://doi.org/10.1016/j.porgcoat.2018.04.012.
667 [47] S.K. Sethi, S. Kadian, R. Gogoi, G. Manik, Layer-by-layer fabrication of self-cleaning
668 superhydrophobic surface made from Carboxymethylcellulose and ZnO quantum dots: A combined
669 experimental and computational study, Surf. Interfaces. 37 (2023) 102752,
670 https://doi.org/10.1016/j.surfin.2023.102752.
671 [48] L.L. Xie, J.H. Chu, X.J. Li, D.N. Zou, L.B. Tong, Improved corrosion resistance of EP
672 coating on Mg alloy through GO hybridization and silica-based superhydrophobic surface, Diam.
673 Relat. Mater. 130 (2022) 109476, https://doi.org/10.1016/j.diamond.2022.109476.
674 [49] Z.X. Xi, C. Tan, L. Xu, Y.Z. Meng, C.Y. Zhang, N. Yang, Q. Li, A novel functional
675 HPPS/PCL/ZnO composite layer on AZ91 for anticorrosion, Mater, Lett. 148 (2015) 134-137,
676 https://doi.org/10.1016/j.matlet.2015.02.056.
677 [50] Y.H. Xie, X.F. Zhou, H.Y. Mi, J.H. Ma, J.Y. Yang, J. Cheng, High efficiency ZnO-based
678 dye-sensitized solar cells with a 1H,1H,2H,2H-perfluorodecyltriethoxysilane chain barrier for
679 cutting on interfacial recombination, Appl. Surf. Sci. 434 (2018) 1144-1152,
680 https://doi.org/10.1016/j.apsusc.2017.11.075.
681 [51] M.A.J. Kouhbanani, S. Mosleh-Shirazi, N. Beheshtkhoo, S. R. Kasaee, S. Nekouian, S.
682 Alshehery, H. Kamyab, S. Chelliapan, M. Azam Ali, A.M. Amani, Investigation through the
683 antimicrobial activity of electrospun PCL nanofiber mats with green synthesized Ag-Fe
684 nanoparticles, J. Drug. Deliv. Sci. Tec. 85 (2023) 104541,
685 https://doi.org/10.1016/j.jddst.2023.104541.

[52] M. Kök, M.E. Pekdemir, E.Ö. Öner, M. C. kun, S. Hekim, MWCNT nanocomposite films prepared using different ratios of PVC/PCL: Combined FT-IR/DFT, thermal and shape memory properties, J. Mol. Struct. 1279 (2023) 134989, https://doi.org/10.1016/j.molstruc.2023.134989.
[53] X.Y. Li, A.X. Lu, H.M. Yang, Structure of ZnO-Fe_2O_3-P_2O_5 glasses probed by Raman and IR spectroscopy, J. Non-Cryst. Solids. 389 (2014) 2-27, http://dx.doi.org/10.1016/j.jnoncrysol.2014.01.051.
[54] H.F. Yang, C.H. Xu, W.M. Wang, P.F. Tang, X.D. Li, S.S. He, H.B. Bao, S.S. Man, D.Y. Tang, X.M. Li, G.C. Yang, Z.Q. Qiao, Underwater self-sustaining combustion and micro-propulsion properties of Al@FAS-17/PTFE-based direct-writing nanothermite, Chem. Eng. J. 451 (2023) 138720, https://doi.org/10.1016/j.cej.2022.138720.
[55] S.L. Chen, M. Yang, Y.Y. Han, H.D. Liu, H.T. Zou, Hydrophobically modified sustainable bio-based polyurethane for controllable release of coated urea, Euro. Polym. J. 142 (2021) 110114, https://doi.org/10.1016/j.eurpolymj.2020.110114.
[56] J.C. Ma, Y.Q. Qing, H.Y. Song, X.J. Cheng, Z.R. Li, C. Long, C.S. Liu, Synergistically coupled double conductive coating-based electronic textiles with superhydrophobic and high-performance strain sensing properties for underwater human motion sensing applications, Chem. Eng. J. 471 (2023) 144284, https://doi.org/10.1016/j.cej.2023.144284.
[57] C.L. Li, Cai Long, Y. Cai, Z.H. Li, Z.Y. Guan, H.Y. Song, L. Guo, X.Y. Xu, C.S. Liu, Y.Q. Qing, Design of amphoteric micro/nanofiber-coupling fabric for ultrafast, precise, and robust removal of water droplets from oils, Chem. Eng. J. 471 (2023) 144479, https://doi.org/10.1016/j.cej.2023.144479
[58] T. Shi, H.N. Wang, Q. Jia, R.Y. Chen, Preparation of a transparent coating with superamphiphobic and antifouling properties, Mater. Chem. Phys. 293 (2023) 126888, https://doi.org/10.1016/j.matchemphys.2022.12688,
[59] Z.L. Wang, A.B. Yang, X.Y. Tan, Y.T. Tu, S. Sabin, P. Xiang, M. Wang, R.H. Guo, X.B. Chen, A veil-over-sprout micro-nano PMMA/SiO2 superhydrophobic coating with impressive abrasion, icing, and corrosion resistance, Colloids. Surface. A. 601 (2020) 1249, https://doi.org/10.1016/j.colsurfa.2020.124998.
[60] Y.X. Bai, H.P. Zhang, J. Zhu, Y.Y. Shao, H. Zhang, A durable superhydrophobic coating based on inherent nano/micro-integrated materials, Prog. Org. Coat. 184 (2023) 107854, https://doi.org/10.1016/j.porgcoat.2023.107854.